ACS OMEGA

http://pubs.acs.org/journal/acsodf

Article

Three-Dimensional Multilayer Vertical Filament Meshes for Enhancing Efficiency in Fog Water Harvesting

Luc The Nguyen, Zhiqing Bai, Jingjing Zhu, Can Gao, Xiaojing Liu, Bewuket T. Wagaye, Jiecong Li, Bin Zhang,* and Jiansheng Guo*

Cite This: *ACS Omega* 2021, 6, 3910−3920

Read Online

ACCESS | Metrics & More | Article Recommendations | Supporting Information

ABSTRACT: Novel types of vertical filament mesh (VFM) fog harvesters, 3D VFM fog harvesters, and multilayer 3D VFM fog harvesters were developed by mimicking the water-harvesting nature of desert beetles and the spider silks from fog. Four different types of polymer filaments with different hydrophilic−hydrophobic properties were used. The polymer filaments were modified with the polyurethane−sodium alginate (PU−SA) mixture solution, and a simple spraying method was used to form alternating 3D PU−SA microbumps. Polymer VFMs exhibited a higher fog-harvesting efficiency than the vertical metal meshes. Moreover, the hydrophobic VFM was more efficient in fog harvesting than the hydrophilic VFM. Notably, the fog-harvesting efficiency of all VFMs increased by 30−80% after spraying with the mixed PU−SA solution to form a 3D geometric surface structure (3D PU−SA microbumps), which mimicked the desert beetle back surface. This modification caused the fog-harvesting efficiency of PTFE 3D VFM to be thrice higher than that of Fe VFM. This increase was attributed to the improved synergistic effects of fog capturing, droplet growing, and droplet shedding. The multilayer VFMs were more efficient in fog harvesting than the single-layer VFMs because of a larger droplet capture area. The fog-harvesting efficiency of two-layer and four-layer polymer VFMs was approximately 35% and about 45% higher than that of the single-layer polymer VFMs, respectively. The four-layer PTFE 3D VFM with the type B PU−SA bump surface (bump/PU−SA) had the highest efficiency of 287.6 mL/m^2/h. Besides the high fog-harvesting efficiency, the proposed polymer VFMs are highly stable, cost-effective, rust-free, and easy to install in practical applications. These advantages are ascribed to the elasticity of the polymer filaments. This work provides new ideas and methods for developing high-performance fog harvesters such as the 3D VFM.

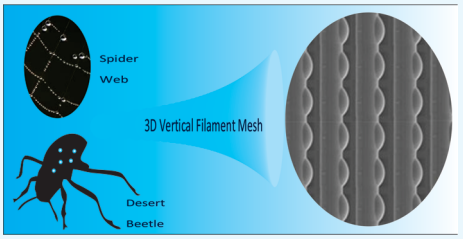

INTRODUCTION

Water is a vital resource for all forms of life. However, the number of people with limited or no access to clean water is on the rise. Similarly, environmental pollution is on the rise. It is, therefore, necessary to develop efficient methods of water harvesting. Researchers have studied many water-harvesting methods in nature by imitating animals and plants such as desert beetles,[1−3] spider silks,[4,5] and cactus plants[6−10] to harvest fog water (fog harvesting). Good potential studies have been realized by mimicking the Namib Desert beetle[7,11,12] and spider silk.[13,14] Various biomimetic methods have been employed to mimic the desert beetle based on the need to improve the materials' surface structure. For example, an improved fog collector was constructed using a weaved superhydrophobic−superhydrophilic patterned fabric followed by the *in situ* deposition of copper particles.[15] The surface containing micro/nanopatterns is prepared by incorporating femtosecond-laser-fabricated polytetrafluoroethylene nanoparticles deposited on the superhydrophobic copper mesh using a pristine hydrophilic copper sheet.[16]

Two main approaches to imitate the spider silk have been explored. The first approach involves designing and preparing beaded fibers with a periodic knots structure through electrospinning to obtain polymer fibers in the form of highly porous membranes.[17,18] The second approach involves immersing a uniform nylon filament into a polymer solution and then drawing it out horizontally using a dip-coater machine. A cylindrical PMMA film forms on the filament surface and spontaneously breaks up into polymer beads because of the Rayleigh instability.[19,20] In these studies, the beetle-imitating bumps were carried out on the sheet or membrane fabric with a metal, polymer, or composite material. The knots appeared continuously on the filament's length and increased the droplet capture capacity and large droplet growth. However, these knots covered the filament's entire circumference, which could lead to a decrease in the droplet shedding efficiency. Nonetheless, only limited studies have been done regarding dynamic factors' effects on fog-harvesting

Received: November 27, 2020
Accepted: January 15, 2021
Published: January 28, 2021

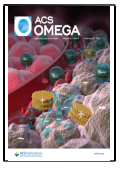

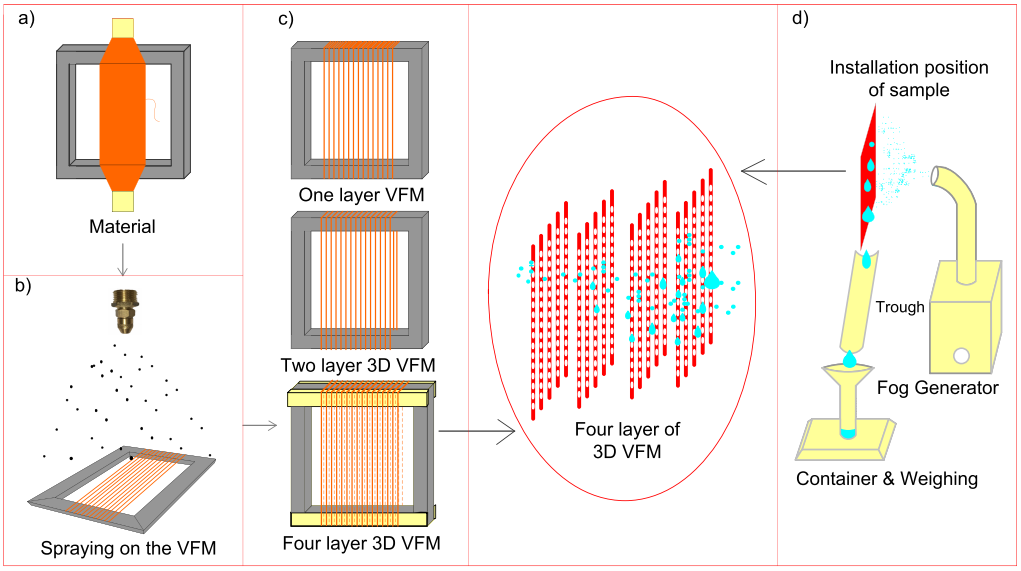

Figure 1. Preparation and measurement of fog-harvesting efficiency of VFM and 3D VFM: (a) preparation of material (polymer filaments, metal wires) and wood frame followed by winding of the filament on the wooden frame (vertical filament mesh); (b) spraying the mixed solution of PU−SA on the filament surface of VFM; (c) representation of the one-layer (single-layer) VFM, two-layer 3D VFM, and four-layer 3D VFM; and (d) schematic diagram of the experimental setup for fog harvesting of VFM.

efficiency (such as Stokes number (St), shade coefficient (SC), etc.).

Recently, W. Shi *et al.* demonstrated a reduction in the droplet clogging and fog-harvesting efficiency of a parallel vertical hydrophilic metal wire system (fog harvesting with harp).[21] A. Sadeghpour *et al.* did a similar study on the droplet condensation behavior of beads using vertical hydrophilic cotton threads.[22] Herein, VFM fog harvesters made of vertical single-layer or multilayer systems containing parallel-arranged polymer filaments (smooth surface) were designed. Four types of single-polymer filaments (monofilaments) with different hydrophilic−hydrophobic properties were used. They included polytetrafluoroethylene (PTFE), polypropylene (PP), polyethylene (PE), and polyamide (PA). It was assumed that they had good ability in capturing water droplets from fog and ease in the sliding down of droplets by gravity based on the understanding of the filaments' properties.

Subsequently, 3D VFM harvesters were fabricated with the hydrophilic bumps (hemispheres) forming part of hydrophobic parallel filaments' surfaces. The system had a well-combined effect of fog capturing, droplet growing, and droplet shedding. Sodium alginate (SA) has good viscosity properties and shapes up easily while bonding with polymers. Polyurethane (PU) has excellent mechanical properties, such as durability and high adhesion. The PU−SA mixture was more hydrophilic and thus caused differences in wettability and surface tension on the surface of hydrophobic materials.[23−27] Polyurethane/sodium alginate based hemisphere microbumps were also created using the simple spray method (similar to the beetles' back surface). The bumps were located alternatively and continuously on the single filament's front surface (similar to the spider silk), which further improved the fog-harvesting efficiency.

EXPERIMENTAL DESIGN AND METHODOLOGY

Materials. The materials used herein were ordered from different companies: 50 wt % polyurethane solution (PU) from H.J. UNKEL Co., Ltd. (Shanghai, China) and sodium alginate powder from Sinopharm Chemical Reagent Co., Ltd. (Shanghai, China). Oil paint (water-based metal antirust paint) was purchased from Guangde Huilong Paint Industry Co., Ltd. (Shanghai, China). Polytetrafluoroethylene (PTFE) was sourced from Dongguan Shengxin Special Rope (ShengXin Special Rope Strap) Co., Ltd. (Dongguan, China), and the thermoplastic polyurethane (TPU) was from the Shenzhen Jietejia Trading (Jitejia Shenzhen Textile Technology) Co., Ltd. (Shenzhen, China). Polyester (PET) and polyamide (PA) were purchased from Shenzhen Yingjie Metallic Yarn Co., Ltd. (Shenzhen, China). Polypropylene (PP) and polyethylene (PE) were purchased from NTEC Monofil Technology Co., Ltd. (Nantong, China). Besides the single filament, there were additional metal wires and materials such as a stretch frame of wooden bars to stratify filaments' layer, glue, and fast absorbent paint.

Fabrication of the Vertical Filament Mesh (VFM) Harvester. The wooden VFM filament stretch frame's internal and external dimensions were 14 × 14 and 18 × 18 cm, respectively. Wooden bars 2 cm wide and 1 cm thick were used to make the frame substrate. A single filament was wound around the frame to enhance the performance and ensure that the filaments were parallel. The separation distance between adjacent filaments ($P = 2D$ and $P = 2.5$ mm) was specified to enable a stable filament tension during use and avoid tangling of adjacent filaments because of the slack. The crossbar of the frame was coated with a layer of paint to make it waterproof and enhance the filaments' distance. A 1 cm thick wooden bar was used for a four-layer sample stuck to the horizontal frame (Figure 1 and Figure S1 in the Supporting Information).

Fabrication of 3D PU−SA Micro Bumps on the Single-Filament Surface. The fabrication of 3D PU−SA microbumps on the single-filament surface was done by dissolving 0.5 g of sodium alginate in 9.5 g of water under a magnetic stirrer for 30 min. This was followed by mixing 100 g of the polyurethane solution and the sodium alginate solution at room temperature for 30 min under a magnetic stirrer to obtain a PU−SA mixture with a 55% concentration. A PU−SA of 40% concentration was obtained using a similar process

https://dx.doi.org/10.1021/acsomega.0c05776
ACS Omega 2021, 6, 3910−3920

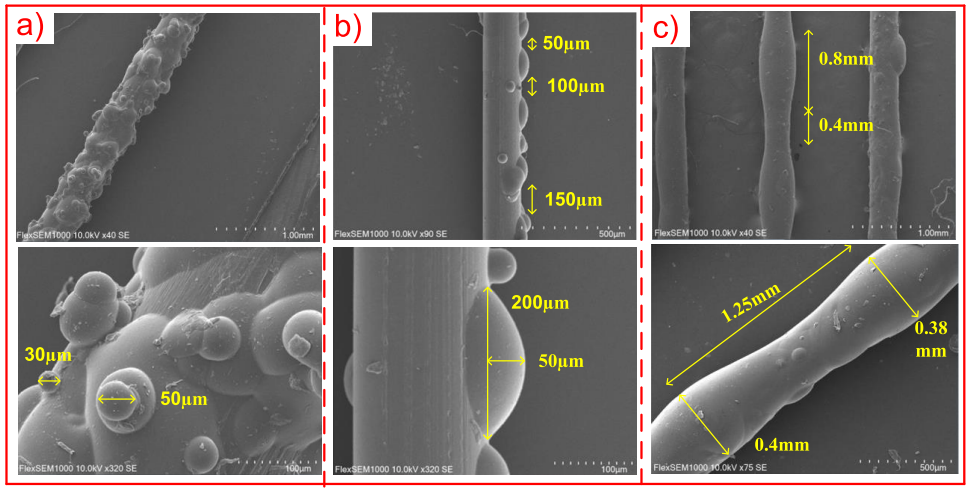

Figure 2. The scanning electron microscope (SEM) image of the microbumps' structure on the single-filament surface: (a) rough/PU−SA (type A), (b) bump/PU−SA (type B), and (c) spindle knot/PU−SA (type C).

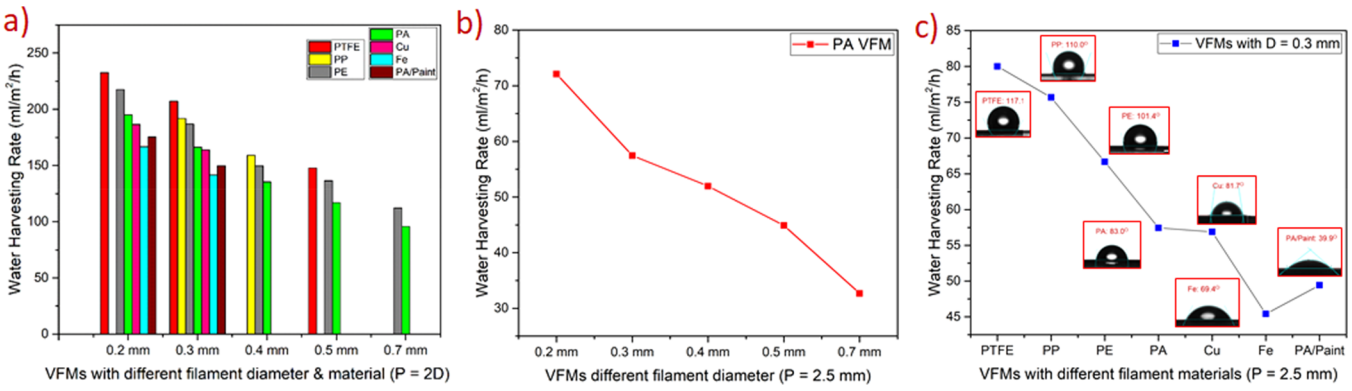

Figure 3. (a) The water-harvesting rate of the VFMs ($P = 2D$) with five different filament diameters and seven different materials. (b) The water-harvesting rate of the PA VFMs with different filament diameters ($P = 2.5$ mm). (c) The water-harvesting rate of the VFMs with six different materials and a filament diameter of 0.3 mm ($P = 2.5$ mm).

(Figure S1 in the Supporting Information). The PU−SA solution was then sprayed on the filament surface using three different methods with two distinct concentrations. The spraying was based on the Rayleigh instability of the fluid membrane breakup,[19,20] and Young's model of surface tension energy and the liquid's contact angle on the solid surface.[28,29] The Laplace pressure differences between the two phases and the curvature of the surface,[30−33] and Furmidge's theory of droplets sliding on a solid surface and spray retention[26] were also factored in. Figure 2 shows the fabrication process for 3D structures on the surface of a single filament. There were three types of 3D geometric structures (3D PU−SA) on the surface of the filaments: type A, rough/PU−SA (Figure 2a); type B, bump/PU−SA (3D PU−SA microbump) (Figure 2b); and type C, spindle knot/PU−SA (Figure 2c) (Figures S1−S3 in the Supporting Information).

The surface of the PA VFM (D = 0.2 and 0.3 mm) was modified with a PA/oil paint to accelerate the sliding of droplets and to improve the fog-harvesting efficiency of VFM. The paint used was more hydrophilic and slippery (lubricated−hydrophilic). It adequately covered the circumference of the filaments. The sample was placed in the laboratory for 24 h, and the fog-harvesting efficiency was measured (Figure S5 in the Supporting Information).[34−38]

Design of the Experimental Setup of the Fog-Harvesting Chamber. An experimental chamber of 2 × 2 × 2 m was set up for the water-harvesting experiment. The temperature of the chamber was maintained at 23 °C with humidity at about 90% using a humidifier. The fog blowing speed and the amount of fog on the sample's surface were also controlled using a portable wind speed meter and humidity measuring instrument, respectively.[39−42] Samples were suspended vertically facing the fog generator at 12 cm and an airflow of 350 mL/h. The volume of collected water was measured after 2 h using an electronic balance (Figure 1d and Figure S1 in the Supporting Information).

Surface Morphology and Optical Contact Angle Measurement. An optical contact angle measuring device (OCA 15EC) was used to measure the different filament materials' static water contact angle. A Panasonic HC-X920M camera was used to record the drop morphology, condensation process of fog drops, movement state, and water droplets' sliding on the mesh. Measurements of the receding and advancing contact angles (θ_r and θ_a) were combined with those of the camera analyzed using the software.[15,21] The FlexSEM 1000-HITACHI SU1000 was used to determine the surface characteristics of VFMs (Figure 2 and Figure S6 in the Supporting Information).

https://dx.doi.org/10.1021/acsomega.0c05776
ACS Omega 2021, 6, 3910−3920

Table 1. Summary of the Water-Harvesting Efficiency of Single Filaments and Wires

single filament/material/parameters		single-filament diameter (D: mm)	contact angle (θ: °)	receding contact angle (θ_r: °)	advancing contact angle (θ_a: °)	$\cos\theta_r - \cos\theta_a$	experimental "critical sliding volume" for droplet (V_e: μL)	shedding rate (droplets/in the first 10′)	volume aggregate in the first 10′: $V_a = V_e{*}N$ (μL)
polytetrafluoroethylene	PTFE	0.2; 0.3; 0.5	117.1	96.1	102.0	0.09	0.91	11	10.01
polypropylene	PP	0.3; 0.4	109.2	92.7	98.1	0.11	1.10	9	9.90
polyethylene PE	PE	0.2; 0.3; 0.4; 0.5; 0.7	101.4	80.6	90.0	0.16	1.40	7	9.80
polyamide	PA	0.2; 0.3; 0.4; 0.5; 0.7	83.0	65.4	84.2	0.32	2.33	4	9.32
copper	Cu	0.2; 0.3	81.7	62.3	80.8	0.31	2.35	4	9.40
steel	Fe	0.2; 0.3	69.4	43.6	70.7	0.39	2.87	3	8.61
PA/oil paint	PA/paint	0.2; 0.3	39.9	23.1	27.6	0.03	0.20	45	9.00
3D VFM	PTFE/PU−SA	0.2; 0.3	90.2	71.2	88.3	0.29	2.44	5	12.21

The values of contact angles and water drop volumes represent averages of three trials. The values of contact angles and uncertainty correspond to ±1−2 standard deviations.

RESULTS AND DISCUSSION

Filament Diameter Influences the VFM's Fog-Harvesting Efficiency. The selection of a suitable filament diameter is an essential factor in structure optimization and improved water-harvesting efficiency of the VFM. Figure 3a ($P = 2D$) and Figure 3b ($P = 2.5$ mm) show the fog-harvesting efficiency of seven kinds of VFMs. The fog-harvesting efficiency increased significantly with the decrease of filament diameter. The water-harvesting rate is a quantity directly related to the efficiency of the overall water harvesting of the VFM. The increase in water-harvesting efficiency between filaments (difference in diameter: 0.1 mm) was approximately 15−20%. The filament's water-harvesting efficiency with a 0.2 mm diameter was about twice that with a 0.7 mm diameter. As such, the efficiency difference for $P = 2.5$ mm between the PA VFM ($D = 0.2$ mm) and PA VFM (0.7 mm) was close to 121% (Supplementary Discussion S2 in the Supporting Information).

The water-harvesting rate is directly correlated with a structure's overall fog collection efficiency,[21,43,44] that is:

$$\eta = \eta_a{}^{*}\,\eta_d,\ \eta_d = S_t/(S_t + \pi/2) \tag{1}$$

$$S_t = \frac{2\rho_{water} v_0 r_{fog}{}^2}{9\mu_{air} R_{filament}} \tag{2}$$

where S_t is the Stokes number, η is the fog-harvesting efficiency, η_a is the aerodynamic efficiency of the wind stream, and η_d is the deposition efficiency of fog droplets suspended in the wind passing through the filaments. ρ_{water} is the density of water, r_{fog} is the fog droplet radius, v_0 is the fog stream velocity, μ_{air} is the air's viscosity, and $R_{filament}$ is the filament radius. Eqs 1 and 2 show that the filament radius is closely related to the Stokes number. A reduced filament radius increases the S_t value, thus increasing the fog-harvesting efficiency of VFMs. Because of this, small-diameter filaments were the preferred choice for improving the efficiency of fog deposition/fog capture efficiency.

The Influence of the Hydrophobic−Hydrophilic Filament in VFM's Fog-Harvesting Efficiency. The surface energy of single-type filaments leads to differences in shapes, water contact angles, advancing contact angle, receding contact angle, and contact angle hysteresis because of the differences in the chemical properties of hydrophobic−hydrophilic structures. These differences result in different fog-harvesting efficiencies. It is therefore important to choose a suitable filament type to improve the fog-harvesting efficiency. An increase in fiber contact angle with water increased the water-harvesting rate (Figure 3a,c). The fog-harvesting efficiency of the polymer VFMs increased in the following order: PA VFM < PE VFM < PP VFM < PTFE VFM. The hydrophobic VFM was more effective in water harvesting than the hydrophilic VFM (Figures 3a,c). At a diameter D of 0.3 mm, the efficiency of hydrophobic VFMs increased by about 12−46% ($P = 2D$) and 16−76% ($P = 2.5$ mm) compared to that of hydrophilic VFM.

The fog-harvesting efficiency of PTFE VFM was 24% ($P = 2D$) and 39% ($P = 2.5$ mm) higher than that of PA VFM. Moreover, the fog-harvesting efficiency of polymer VFM harvesters was higher or equivalent to that of metal vertical wire meshes at both filament distances ($P = 2D$ and $P = 2.5$ mm) (Figure 3a,c). The fog-harvesting efficiencies of the copper vertical wire mesh and PA VFM in both distance categories ($P = 2D$ and $P = 2.5$ mm) were equivalent but lower than those of all other polymer VFM harvesters. Notably, the water-harvesting efficiency of PTFE VFM was approximately 46−76% higher than that of Fe VFM (Supplementary Discussion S2 in the Supporting Information).

These results are consistent with the theory of Kawasaki and Furmidge and the study done by Weiwei Shi. The effective drainage of the droplets down the VFMs is quantified using a contact angle hysteresis model. Theoretically, the critical volume (Vc,t) required for a droplet to slide down the wire is approximated as:[21,26,45−49]

$$\rho_{water} g V_t = \pi R_f \gamma(\cos\theta_r - \cos\theta_a) \tag{3}$$

where ρ_{water} is the density of water, g is the gravitational acceleration constant, V_t is the theoretically obtained critical sliding volume, R_f is the radius of the filament, γ is the surface tension of the liquid, θ_a is the advancing contact angle, and θ_r is the receding contact angle.

In eq 2, ρ_{water}, g, and π are constant values. As such, the value of V_t depends on the values of γ and $\cos\theta_r - \cos\theta_a$ at the same filament diameter. An increase in $\cos\theta_r - \cos\theta_a$ causes an increase in V_t and vice versa. Substituting eq 2 with the values of $\cos\theta_r - \cos\theta_a$ in Table 1 produces the results. Comparing the V_t values of different filaments, the order of magnitude is:

$$V_{t(PTFE)} < V_{t(PP)} < V_{t(PE)} < V_{t(PA)} \leq V_{t(Cu)} < V_{t(Fe)}$$

https://dx.doi.org/10.1021/acsomega.0c05776
ACS Omega 2021, 6, 3910−3920

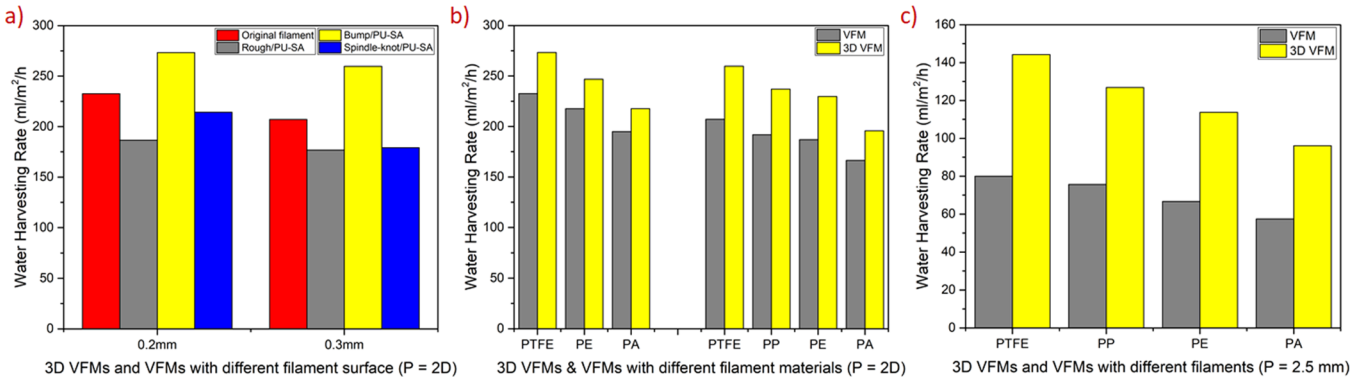

Figure 4. (a) Comparison of the water-harvesting rate of the PTFE VFM (P = 2D; D = 0.2 and 0.3 mm) with three types of filament surface geometry structures (rough/PU−SA (type A), bump/PU−SA (type B), and spindle knot/PU−SA (type C)). (b) Comparison of the water-harvesting rate of the 3D VFMs with the VFMs (D = 0.2 and 0.3 mm; P = 2D). (c) Comparison of the water-harvesting rate of the 3D VFMs and the VFMs (D = 0.3 mm; P = 2.5 mm).

If the static contact angle values (Table 1) are filled in Young's model eq 1 ($\gamma_{SV} = \gamma_{LV} \cos\theta + \gamma_{SL}$), the comparable results of the surface tension energy (γ) of the single filaments are:

$$\gamma_{(PTFE)} < \gamma_{(PP)} < \gamma_{(PE)} < \gamma_{(PA)} < \gamma_{(Cu)} < \gamma_{(Fe)}$$

These results are consistent with those obtained after comparing the theoretically obtained critical sliding volume V_t. The smaller the volume, the higher the drainage efficiency of the droplets. As such, the drainage level of VFM in ascending order is:

PTFE > PP > PE > PA > Cu > Fe

These initial results demonstrated that most hydrophobic VFMs (within this study's scope) had a high effective drainage of droplets and a higher fog-harvesting efficiency than hydrophilic VFMs. In the same line, the effective drainage of droplets in PA/oil paint VFM (lubricated−hydrophilic) was high despite it having a low water-harvesting efficiency(its causes are discussed in the subsequent sections). These results will be the basis for choosing a suitable filament type based on 3D VFM fabrication to obtain the optimum efficiency.

The Filament Surface Morphology Affected the Water-Harvesting Efficiency of the 3D VFM. The water-harvesting rate of 3D VFM type B (bump/PU−SA) was higher than that of 3D VFM type A (rough/PU−SA), 3D VFM type C (spindle knot/PU−SA), and VFM (Figure 4a). The water-harvesting rate of the 3D VFM with P = 2D increased by approximately 12−25% compared to that of VFM (Figure 4b). Notably, the difference in the water-harvesting rate between 3D PTFE VFM and the original PTFE VFM with P = 2.5 mm was approximately 80% (Figure 4c). The water-harvesting rate of 3D PTFE VFM was the highest (273.3 mL/m^2/h) (Supplementary Discussion S2 in the Supporting Information). Nonetheless, the water-harvesting rate of the hydrophobic 3D VFM was higher than that of the hydrophilic 3D VFM.

The fog-harvesting efficiency of 3D VFM with bump/PU−SA was affected by several factors. One factor was the solid surface's heterogeneous wettability, which caused the "driving force F_w" to appear. The F_w is expressed by eq 4[30,50−53] as:

$$F_w = \pi R_d \gamma(\cos\theta_M - \cos\theta_L) \quad (4)$$

where R_d is the droplet's radius, γ is the surface tension, and θ_L and θ_M are the contact angles at the less wettable and more wettable side of the droplet, respectively (Figures 5b,d). The

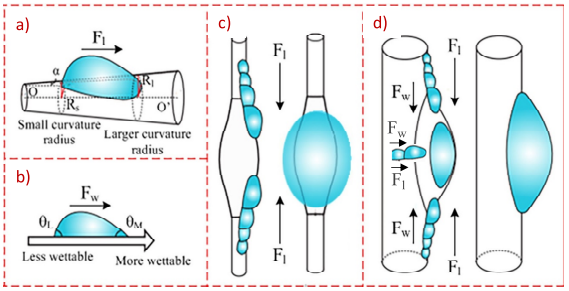

Figure 5. (a) Driving force generated by the shape gradient (F_l) propels liquid droplets toward the region with a larger curvature radius. (b) Driving force generated by surface wettability gradient (F_w) propels liquid droplets toward the wetter region (adapted from ref 30. Copyright 2014 American Chemical Society). (c) Driving forces of the directional movement of droplets on the surface of vertical cylindrical filament with spindle knots. (d) Driving forces of the directional movement of droplets on the surface of the vertical filament with bumps.

fog droplets spread quickly and formed large droplets upon contacting the hydrophilic PU−SA bumps. However, the fog droplets contacting the non-PU−SA-coated filament area with a more hydrophobic surface condensed rapidly and moved simultaneously toward the more hydrophilic PU−SA bumps. This phenomenon was attributed to the F_w force. These findings were consistent with those of Shuai Yang *et al.* The study revealed that antigravity water transport could spontaneously transport water from the lower hydrophobic side to the upper superhydrophilic side without an input of external energy. The water droplets would continue to merge with the larger droplets on the hydrophilic PU−SA bumps (the hydrophilic and millimeter-scale bumps are great for increasing the diffusional flux of water vapor), thus accelerating the growth of the large droplets.[54] This phenomenon was similar to the water-droplet-capturing behavior of desert beetle backs. The findings confirmed the effectiveness of 3D VFM in water droplet capture and droplet growth ability.

The second factor was based on eq 5:[30,55−60]

$$F_l = \int_{R_s}^{R_l} \frac{2\gamma}{(R + R_d)^2} \sin\alpha \, dz \quad (5)$$

where R is the local radius of the cone-structured object, R_d is the radius of the droplet, R_s and R_l are the local radii of the

https://dx.doi.org/10.1021/acsomega.0c05776
ACS Omega 2021, 6, 3910−3920

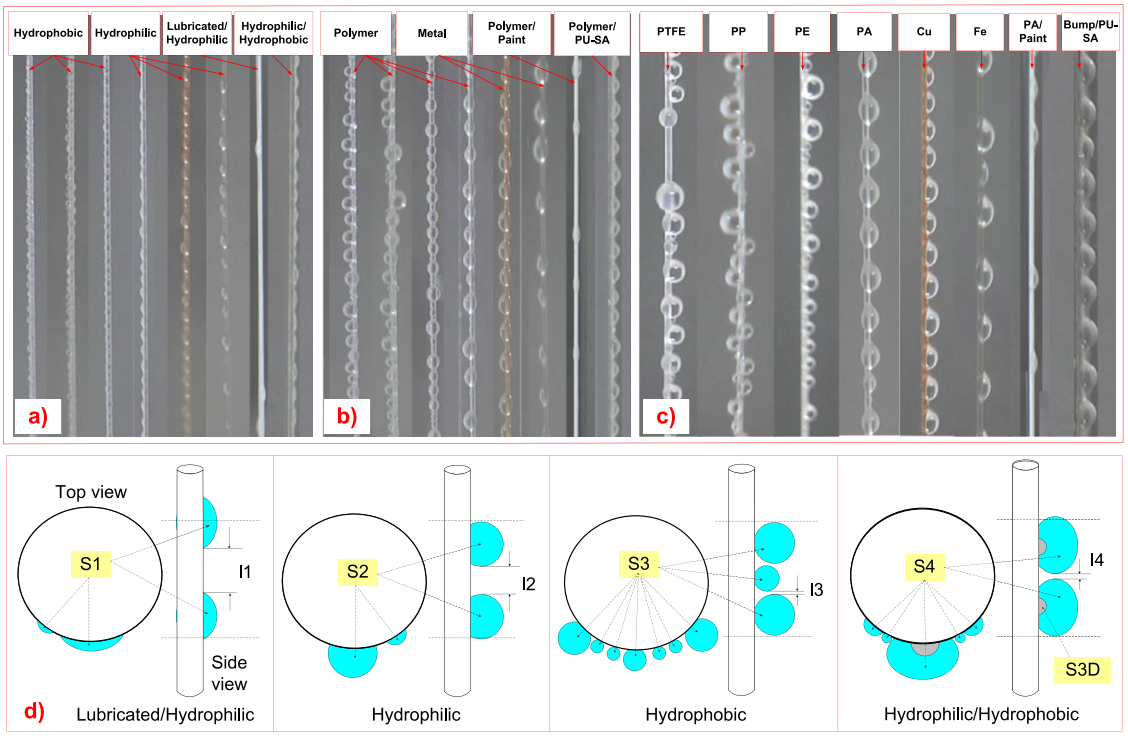

Figure 6. Illustration of the state, shape, and size of water droplets on different VMFs at different times (D = 0.3 mm; P = 2.5 mm): (a) the first 30 s; (b) the first 60 s; (c) the time for large droplets to reach the critical sliding volume before it starts to slide down; (d) illustration of the side and top views: S1, S2, S3, and S4 are new 3D droplet capture areas of the lubricated−hydrophilic filament, hydrophilic filament, hydrophobic filament, and hydrophilic/hydrophobic filament (bump/PU−SA filament) in the same length segment (h) on the vertical filament surface, respectively. S3D is the original droplet capture area of the bump/PU−SA filament surface. $L1$, $l2$, $l3$, and $l4$ are the distance between adjacent droplets of the lubricated−hydrophilic filament, hydrophilic filament, hydrophobic filament, and hydrophilic/hydrophobic filament, respectively.

object at the two opposite sides of the droplet, α is the half apex angle of the cone, and dz is the minute incremental radius along the cone (Figure 5a,c,d).

The pressure difference was caused by differences in radius (shape gradient) on the bump surface and the positions of PU−SA bumps on the filament surface. These differences caused the Laplace force to propel liquid droplets toward the region with a larger curvature radius. The Laplace force could accelerate the movement of droplets and the growth of large droplets (Figures 5a,d). These findings were consistent with the study results of Junrui Wu *et al.*, which reported that the prepared sample spontaneously and directionally moved the water droplets from the minor side to the large side of the trapezoidal platform surface.[61] It was also similar to the act of capturing waterdrops in the spider silk. This finding further confirmed the effectiveness of 3D VFM in water droplet capture and droplet growth.

The third factor was the wettable filament surface structure, the shape of the droplet, and condensing on the hydrophilic cotton thread's yarn surface, also known as bead coalescence.[22] Differences in the size, shape, and distribution of water droplets on the filament surface affected the droplets' capture area and capture efficiency (Figure 6). The dropped fog rapidly formed very small round droplets on multiple sides of the filament surface (front, left, and right with a dense covering) upon contacting the hydrophobic VFM surface. Based on the theory of surface tension and Young's model, water contacting the surface of lower-surface-energy materials (hydrophobic materials) would shrink rapidly and form a round thick water droplet. Herein, the static contact angle, advancing contact angle, and receding contact angle were large (Table 1). They then grew up to form large and small round droplets alternating continuously. The distance between the droplets was very short, $l3 = 0-0.5D$. This phenomenon caused a "new 3D surface area (S3 is large)/new 3D droplet capture area" to rapidly form on the surface of the filament, which was larger than the "original filament surface area." The area had lots of very small round water droplets that appeared during the first 30 s. (Figure 6c,d). This occurrence caused the capturing ability of new droplets to increase. The increase was attributed to two reasons: increased surface area and better droplet absorption on the surface of water droplets than the filament itself ("droplets capture droplets").

The fog drops spread rapidly and formed water droplets in long and long−thin shapes upon contacting the surface of the hydrophilic VFM and lubricated−hydrophilic VFM (Figure 6). The droplets ($l1$, $l2 = 2-6D$) were larger than those of the hydrophobic group. A long−thin water membrane continuously formed, covering the hydrophilic VFM before forming the large droplet. The water droplets created the S1 and S2 on the hydrophilic VFM surface and lubricated−hydrophilic VFM surface, respectively (S1 < S2 < S3). These findings implied that the droplet capture effect of the hydrophilic VFM and lubricated−hydrophilic VFM was lower than that of hydrophobic VFM.

The 3D PTFE VFM had an added advantage of the 3D surface area of the bump (S3D). It was, therefore, capable of enhancing the advantages of both hydrophobic and hydrophobic surfaces. The thick round droplets still formed on the original filament area part of the hydrophobic PTFE (not coated with the PU−SA solution) to increase the new droplet capture area. These droplets also moved toward the bump. The

https://dx.doi.org/10.1021/acsomega.0c05776
ACS Omega 2021, 6, 3910−3920

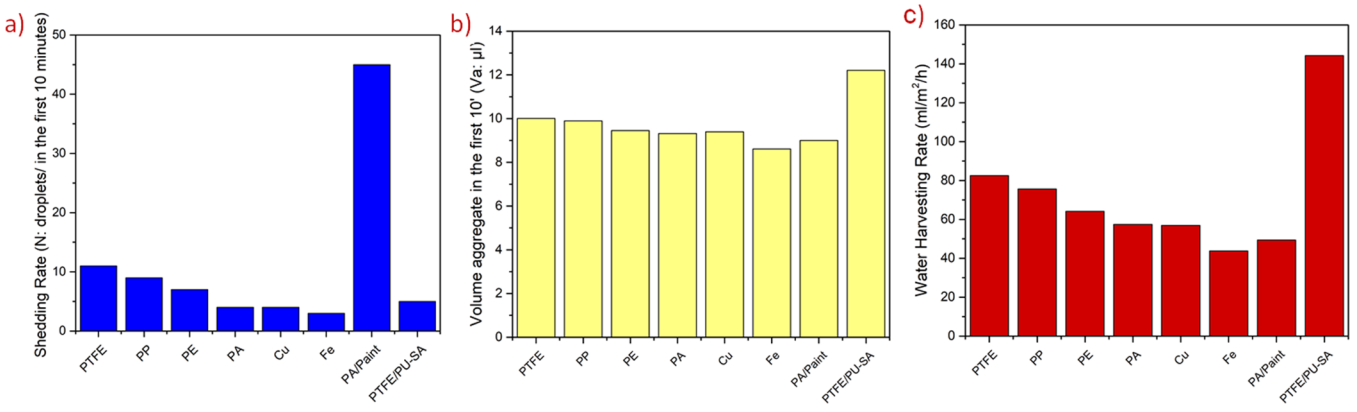

Figure 7. (a) The number of droplets that slid down the VFM in the first 10 min (D = 0.3 mm; $P = 2D$). (b) The overall water volume poured into the container after the first 10 min. (c) The water-harvesting rate of 3D PTFE VFM (PTFE/PU−SA) and VFMs.

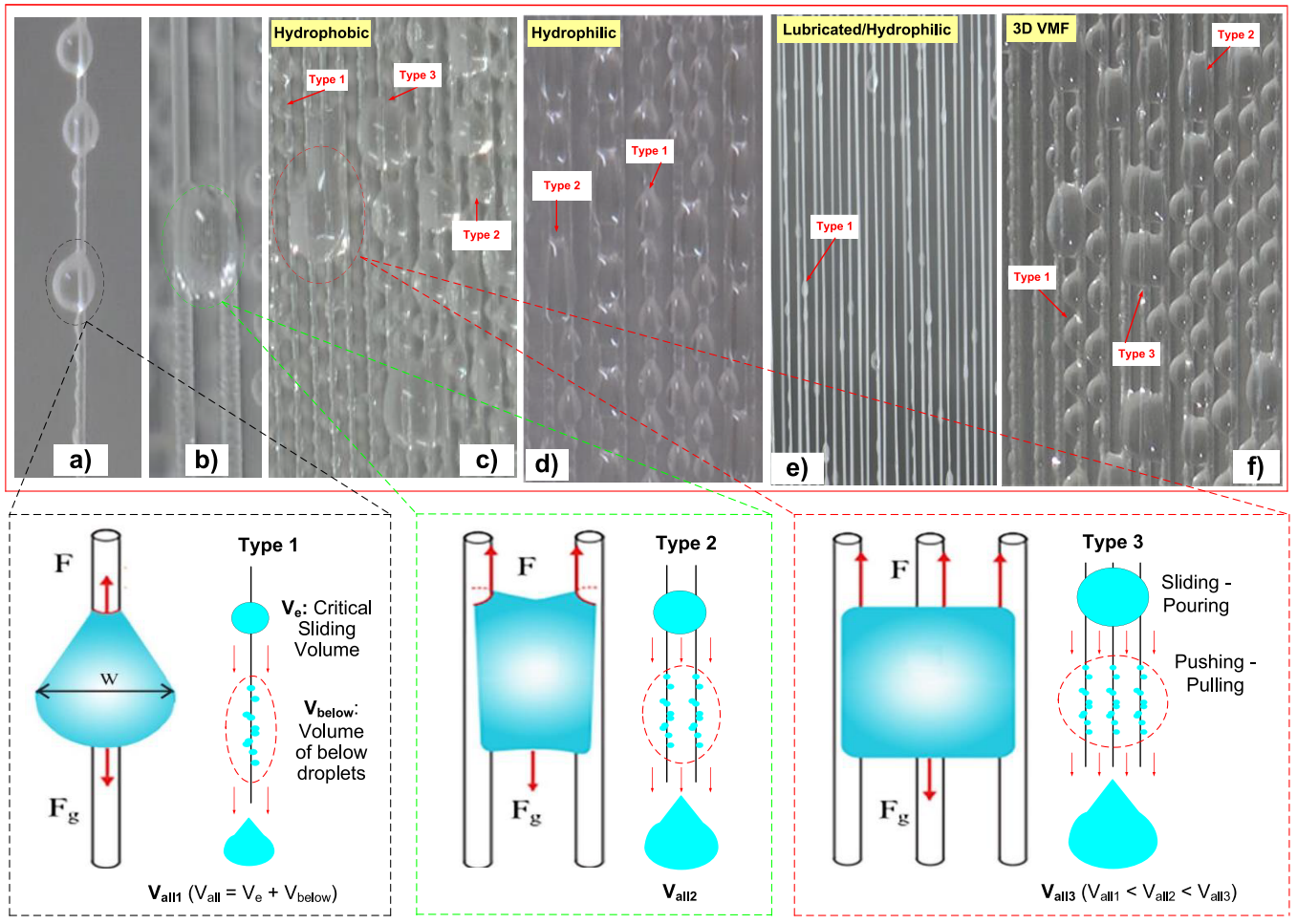

Figure 8. Illustration of droplet shapes on the different VFMs (D = 0.3 mm; $P = 2D$): (a) A droplet sliding down from one side of a vertical filament ($w/2 < P - R_f$, P is the center-to-center spacing between adjacent filaments, R_f is the radius of the filament); type 1. (b) A droplet sliding down between two adjacent vertical filaments ($w/2 > P - R_f$); type 2. (c) A liquid filmlike droplet sliding down along three adjacent vertical filaments ($w/2 >> P - R_f$); type 3. Droplet shape on the hydrophobic VFM, where w is the width of the droplet, F_g is the gravity force, and F is the retention force of the liquid on the solid (reproduced from ref 21. Copyright 2018 American Chemical Society). (d) Droplet shapes on the hydrophilic VFM. (e) Droplet shapes on the lubricated−hydrophilic VFM. (f) Droplet shapes on the 3D VMF.

droplets on the bump/PU−SA also quickly formed to create a new droplet capture area surface: S4 > S3 > S2 > S1. The distance between the droplets was $l4 = 0-0.5D$ (Figure 6c). It was possibly the reason why the 3D VFM had a superior water-harvesting efficiency compared to FM.

The fourth factor that could have caused the droplet capture area to be effective was the efficient droplet pouring process of the 3D VFM. The process had commendable rates of critical droplet sliding down (shedding rate) per unit time (N), critical sliding volume (V_e), and the overall water volume poured into

https://dx.doi.org/10.1021/acsomega.0c05776
ACS Omega 2021, 6, 3910−3920

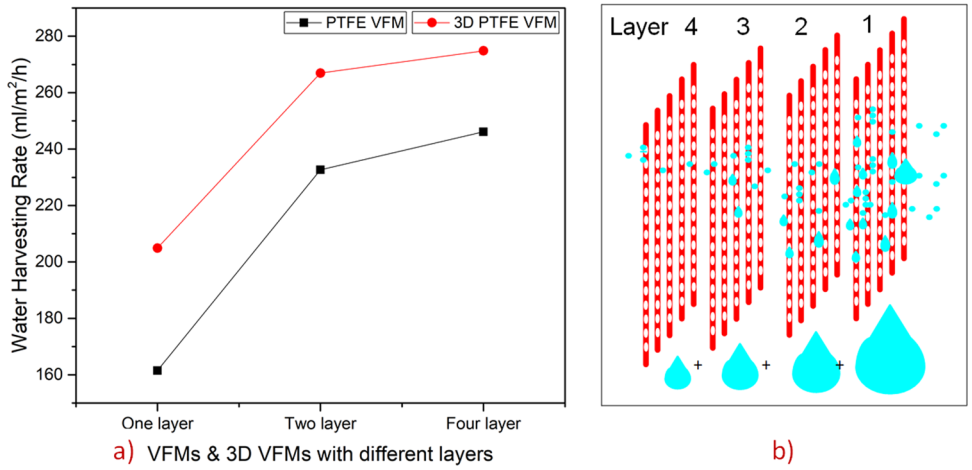

Figure 9. (a) Comparison of the water-harvesting efficiency of multilayer VFMs and multilayer 3D VFMs. (b) Illustration of the fog flow impact with layers of VFM and 3D VFM.

the container after a critical droplet had slid down (V_a and V_{all}) (Figure 7).

Although the shedding rate of 3D VFM was higher than that of Fe VFM, PA VFM, and Cu VFM, it was lower than that of hydrophobic VFM and the lubricated−hydrophilic VFM (Figure 7a). However, the overall water volume poured into the container during the first 10 min (P = 2.5 mm) in 3D VFM was much higher than that in other VFMs (Figure 7b). Figure 7c shows the superior water-harvesting efficiency of 3D VFM compared to VFM. Notably, the water-harvesting efficiency of 3D PTFE VFM was about thrice that of Fe VFM (Supplementary Discussion S2 in the Supporting Information).

Efficient droplet pouring was further demonstrated by the overall water volume poured into the container after a critical droplet had slid down (V_{all}) (P = 2D) (Figure 8).

The lubricated−hydrophilic VFM appeared only as droplets type 1 in the case of P = 2D. The hydrophilic VFM appeared in many types of drops 1 and 2. The 3D VFM and hydrophobic VFM appeared as many types of drops 2 and 3. Based on eqs 3, 6, and 7,[21,26,45−49] the shedding rate of large droplets of type 3 was slower than that of types 1 and 2.

$$\rho_{water} g V_t = 2\pi R_f \gamma(\cos\theta_r - \cos\theta_a) \quad (6)$$

$$\rho_{water} g V_t = 3\pi R_f \gamma(\cos\theta_r - \cos\theta_a) \quad (7)$$

However, when large droplets (V_e) of type 3 slid down, they spread to a wider area and slid down together with the below droplets (V_{below}). As such, the overall water volume poured into the container after a critical droplet had slid down (V_{all}) in the 3D VFM was very high. This phenomenon caused the fog-harvesting efficiency of the 3D VFMs to be higher than that of VFMs.

In type A rough/PU−SA, the fog-harvesting efficiency of the 3D VFM decreased compared to that of the original VFM. This decrease was attributed to the filament surface coating with the smallest size (about 30−100 μm) of PU−SA droplet overlapping layer, which led to an increase in filament diameter. Eq 2 demonstrates that the Stokes number decreased with an increase in the filament diameter, which reduced the water-harvesting efficiency.

In type C, the Laplace force propelled the water droplets toward the region with a larger curvature radius, thus promoting growth (eq 5). However, the whole filament surface had been coated by hydrophilic PU−SA, causing the fiber diameter to increase. This increase caused the large droplets to converge because of the lack of F_w force. Large droplets took longer to form and reach the critical sliding volume, thus reducing the water drainage efficiency of 3D VFM.

These findings revealed that the hydrophilic−hydrophobic properties of the VFM and 3D VFM should balance between fog capturing, droplet growing, and droplet shedding to achieve a higher fog-harvesting efficiency. There were four typical cases for this complex relationship: PTFE VFM, Fe VFM, PA/paint VFM, and 3D PTFE VFM. Nonetheless, the shedding rate of PA/paint VFM was superior. In PA/paint VFM, the water volume that poured into the container after a critical droplet slid down was not high. As such, the efficiency of harvesting water was not high. In contrast, the critical sliding volume of Fe VFM was large but with a low shedding rate. PTFE VFM had an effective drainage efficiency and effective droplet pouring. Notably, the 3D PTFE VFM effectively worked out this compromise by significantly improving the fog-harvesting efficiency. This improvement was attributed to the enhanced synergistic effects of fog capturing, droplet growing, and droplet shedding.

The Filament Multilayer and the Water Harvesting of the VFM and 3D VFM. The efficiency of the double-layer polymer VFM was 34% higher than that of the single-layer polymer VFM (Figure 9). In the same line, the efficiency of the four-layer polymer VFM was 46% higher than that of the single-layer polymer VFM. The four-layer polymer VFM with a 3D bump surface (PU−SA) had the highest efficiency of 287.6 mL/m^2/h (Supplementary Discussion S2 in the Supporting Information).

The main reason for the improved efficiency was the modified filaments with small diameters similar to the beetle's dorsal surface (the bump is only on the front part of the fiber diameter circumference). These modifications enhanced the deposition efficiency (high Stokes number) based on eqs 1 and 2. The multilayered structure increased the droplet capture area, which enhanced the fog capture efficiency (Figure 8b). These attributes led to the high efficiency of the multilayer 3D VMF compared to the findings of Musaddaq Azeem *et al.*[62,63]

https://dx.doi.org/10.1021/acsomega.0c05776
ACS Omega 2021, 6, 3910−3920

CONCLUSIONS

Polymer VFMs exhibited a higher fog-harvesting efficiency than the vertical metal meshes because of the efficient fog capturing and rapid droplet sliding down (droplet shedding). Nonetheless, the hydrophobic VFM was more efficient in fog harvesting than the hydrophilic VFM. The fog-harvesting efficiency of all VFMs increased after spraying the mixed solution of PU−SA and forming a 3D geometric surface structure (3D PU−SA microbumps) to mimic the desert beetle back surface. The increment of fog-harvesting efficiency was about 30−80%. It was attributed to the improved synergistic effects of fog capturing, droplet growing, and droplet shedding. The multilayer VFMs were more efficient in fog harvesting than the single-layer VFMs because of a larger droplet capture area. The fog-harvesting efficiency of two-layer and four-layer polymer VFMs was approximately 35% and about 45% higher than that of the single-layer polymer VFMs, respectively. The four-layer PTFE 3D VFM with type B PU−SA bumps surface (bump/PU−SA) had the highest efficiency of 287.6 mL/m^2/h. Besides the high fog-harvesting efficiency, the proposed polymer VFMs are highly stable, cost-effective, rust-free, and easy to install in practical applications. These advantages are ascribed to the elasticity of the polymer filaments. This work provides new ideas and methods for developing high-performance fog harvesters such as the 3D VFM.

ASSOCIATED CONTENT

Supporting Information

The Supporting Information is available free of charge at https://pubs.acs.org/doi/10.1021/acsomega.0c05776.

Image of the abstract section (novel types of vertical filament mesh (VFM) fog harvesters, 3D VFM fog harvesters, and multilayer 3D VFM fog harvesters were developed by mimicking the water-harvesting nature of desert beetles and the spider silk from fog); dimension of frame and installation position of the sample; preparation of 3D PU−SA microbumps' structure on the single-filament surface; detailed description of the spray method on a single filament of vertical filament mesh; FTIR of polyurethane−sodium alginate (PU−SA) and paint/oil (Figures S1−S6); and test results table for the water-harvesting rate of VFM and 3D VFM (Tables S1−S5) (PDF)

Recording a part of the fog-harvesting process for the 3D VFM harvester (Movie S1) (MP4)

AUTHOR INFORMATION

Corresponding Authors

Bin Zhang − *Key Laboratory of Textile Science and Technology, Ministry of Education, College of Textiles, Donghua University, Shanghai 201620, China*; Email: zhangbin@dhu.edu.cn

Jiansheng Guo − *Key Laboratory of Textile Science and Technology, Ministry of Education, College of Textiles, Donghua University, Shanghai 201620, China*; orcid.org/0000-0002-8905-7040; Email: jsguo@dhu.edu.cn

Authors

Luc The Nguyen − *Key Laboratory of Textile Science and Technology, Ministry of Education, College of Textiles, Donghua University, Shanghai 201620, China; Faculty of Garment Technology and Fashion Design, Hung Yen University of Technology and Education, Hai Duong 170000, Vietnam*

Zhiqing Bai − *Key Laboratory of Textile Science and Technology, Ministry of Education, College of Textiles, Donghua University, Shanghai 201620, China*

Jingjing Zhu − *Key Laboratory of Textile Science and Technology, Ministry of Education, College of Textiles, Donghua University, Shanghai 201620, China*

Can Gao − *Key Laboratory of Textile Science and Technology, Ministry of Education, College of Textiles, Donghua University, Shanghai 201620, China*

Xiaojing Liu − *Key Laboratory of Textile Science and Technology, Ministry of Education, College of Textiles, Donghua University, Shanghai 201620, China*

Bewuket T. Wagaye − *Key Laboratory of Textile Science and Technology, Ministry of Education, College of Textiles, Donghua University, Shanghai 201620, China*

Jiecong Li − *Key Laboratory of Textile Science and Technology, Ministry of Education, College of Textiles, Donghua University, Shanghai 201620, China*

Complete contact information is available at: https://pubs.acs.org/10.1021/acsomega.0c05776

Author Contributions

The manuscript was written through the contribution of all authors. All authors have given approval to the final version of the manuscript.

Notes

The authors declare no competing financial interest.

ACKNOWLEDGMENTS

This work was supported by the earmarked fund for China Agriculture Research System for Bast and Leaf Fiber Crops (grant number CARS-16).

REFERENCES

(1) Mondal, B.; Mac Giolla Eain, M.; Xu, Q.; Egan, V. M.; Punch, J.; Lyons, A. M. Design and Fabrication of a Hybrid Superhydrophobic-Hydrophilic Surface That Exhibits Stable Dropwise Condensation. *ACS Appl. Mater. Interfaces* **2015**, *7*, 23575−23588.

(2) Ahmad, Z.; Ahmad, I.; Patel, F. Fog Collection by Mimicking Nature. *J. Biomimetics, Biomater., Tissue Eng.* **2010**, *8*, 35−43.

(3) Hunter, P. Turning nature's inspiration into a production line. *EMBO Rep.* **2014**, *15*, 1123−1127.

(4) Bai, H.; Ju, J.; Sun, R.; Chen, Y.; Zheng, Y.; Jiang, L. Controlled Fabrication and Water Collection Ability of Bioinspired Artificial Spider Silks. *Adv. Mater.* **2011**, *23*, 3708−3711.

(5) Ganesh, V. A.; Ranganath, A. S.; Baji, A.; Raut, H. K.; Sahay, R.; Ramakrishna, S. Hierarchical Structured Electrospun Nanofibers for Improved Fog Harvesting Applications. *Macromol. Mater. Eng.* **2017**, *302*, 1600387.

(6) Gürsoy, M.; Harris, M. T.; Downing, J. O.; Barrientos-Palomo, S. N.; Carletto, A.; Yaprak, A. E.; Karaman, M.; Badyal, J. P. S. Bioinspired fog capture and channel mechanism based on the arid climate plant Salsola crassa. *Colloids Surf., A* **2017**, *529*, 195−202.

(7) Brown, P. S.; Bhushan, B. Bioinspired materials for water supply and management: water collection, water purification and separation of water from oil. *Philos. Trans. R. Soc., A* **2016**, 20160135.

(8) Gurera, D.; Bhushan, B. Designing bioinspired surfaces for water collection from fog. *Philos. Trans. R. Soc., A.* **2019**, *377*, 20180269.

(9) Cao, M.; Ju, J.; Li, K.; Dou, S.; Liu, K.; Jiang, L. Facile and Large-Scale Fabrication of a Cactus-Inspired Continuous Fog Collector. *Adv. Funct. Mater.* **2014**, *24*, 3235−3240.

(10) Tan, X.; Shi, T.; Tang, Z.; Sun, B.; Du, L.; Peng, Z.; Liao, G. Investigation of Fog Collection on Cactus-inspired Structures. *J. Bionic Eng.* **2016**, *13*, 364−372.
(11) Xu, C.; Feng, R.; Song, F.; Wang, X.-L.; Wang, Y.-Z. Desert Beetle-Inspired Superhydrophilic/Superhydrophobic Patterned Cellulose Film with Efficient Water Collection and Antibacterial Performance. *ACS Sustainable Chem. Eng.* **2018**, *6*, 14679−14684.
(12) Garrod, R. P.; Harris, L. G.; Schofield, W. C. E.; McGettrick, J.; Ward, L. J.; Teare, D. O. H.; Badyal, J. P. S. Mimicking a Stenocara Beetle's Back for Microcondensation Using Plasmachemical Patterned Superhydrophobic-Superhydrophilic Surfaces. *Langmuir* **2007**, *23*, 689−693.
(13) Chen, Y.; Zheng, Y. Bioinspired micro−/nanostructure fibers with a water collecting property. *Nanoscale* **2014**, *6*, 7703−7714.
(14) Hou, Y.; Chen, Y.; Xue, Y.; Wang, L.; Zheng, Y.; Jiang, L. Stronger water hanging ability and higher water collection efficiency of bioinspired fiber with multi-gradient and multi-scale spindle knots. *Soft Matter* **2012**, *8*, 11236.
(15) Yu, Z.; Zhang, H.; Huang, J.; Li, S.; Zhang, S.; Cheng, Y.; Mao, J.; Dong, X.; Gao, S.; Wang, S.; Chen, Z.; Jiang, Y.; Lai, Y. Namib desert beetle inspired special patterned fabric with programmable and gradient wettability for efficient fog harvesting. *J. Mater. Sci. Technol.* **2021**, *61*, 85−92.
(16) Yin, K.; Du, H.; Dong, X.; Wang, C.; Duan, J.-A.; He, J. A simple way to achieve bioinspired hybrid wettability surface with micro/nanopatterns for efficient fog collection. *Nanoscale* **2017**, *9*, 14620−14626.
(17) Dong, H.; Wang, N.; Wang, L.; Bai, H.; Wu, J.; Zheng, Y.; Zhao, Y.; Jiang, L. Bioinspired electrospun knotted microfibers for fog harvesting. *ChemPhysChem* **2012**, *13*, 1153−1156.
(18) Thakur, N.; Ranganath, A. S.; Agarwal, K.; Baji, A. Electrospun Bead-On-String Hierarchical Fibers for Fog Harvesting Application. *Macromol. Mater. Eng.* **2017**, *302*, 1700124.
(19) Song, Y.-y.; Liu, Y.; Jiang, H.-b.; Li, S.-y.; Kaya, C.; Stegmaier, T.; Han, Z.-w.; Ren, L.-q. Bioinspired Fabrication of one dimensional graphene fiber with collection of droplets application. *Sci. Rep.* **2017**, *7*, 12056.
(20) Chen, Y.; Wang, L.; Xue, Y.; Jiang, L.; Zheng, Y. Bioinspired tilt-angle fabricated structure gradient fibers: micro-drops fast transport in a long-distance. *Sci. Rep.* **2013**, *3*, 2927.
(21) Shi, W.; Anderson, M. J.; Tulkoff, J. B.; Kennedy, B. S.; Boreyko, J. B. Fog Harvesting with Harps. *ACS Appl. Mater. Interfaces* **2018**, *10*, 11979−11986.
(22) Sadeghpour, A.; Zeng, Z.; Ji, H.; Dehdari Ebrahimi, N.; Bertozzi, A. L.; Ju, Y. S. Water vapor capturing using an array of traveling liquid beads for desalination and water treatment. *Sci. Adv.* **2019**, *5*, No. eaav7662.
(23) Tang, Y.; Yang, J.; Yin, L.; Chen, B.; Tang, H.; Liu, C.; Li, C. Fabrication of superhydrophobic polyurethane/MoS_2 nanocomposite coatings with wear-resistance. *Colloids Surf., A* **2014**, *459*, 261−266.
(24) Zeng, X.; Qian, L.; Yuan, X.; Zhou, C.; Li, Z.; Cheng, J.; Xu, S.; Wang, S.; Pi, P.; Wen, X. Inspired by Stenocara Beetles: From Water Collection to High-Efficiency Water-in-Oil Emulsion Separation. *ACS Nano* **2017**, *11*, 760−769.
(25) Liu, H.; Gao, S.-W.; Cai, J.-S.; He, C.-L.; Mao, J.-J.; Zhu, T.-X.; Chen, Z.; Huang, J.-Y.; Meng, K.; Zhang, K.-Q.; Al-Deyab, S. S.; Lai, Y.-K. Recent Progress in Fabrication and Applications of Superhydrophobic Coating on Cellulose-Based Substrates. *Materials* **2016**, *9*, 124.
(26) Furmidge, C. G. L. Studies at phase interfaces I. the sliding of liquid drops on solid surfaces and a theory for spray retention. *J. Colloid Sci.* **1962**, *17*, 309−324.
(27) Wang, X.; Zeng, J.; Yu, X.; Zhang, Y. Superamphiphobic coatings with polymer-wrapped particles: Enhancing water harvesting. *J. Mater. Chem. A* **2019**, *7*, 5426−5433.
(28) Lafuma, A.; Quéré, D. Superhydrophobic states. *Nat. Mater.* **2003**, *2*, 457−460.
(29) Park, S.; Kim, J.; Park, C. H. Superhydrophobic Textiles: Review of Theoretical Definitions, Fabrication and Functional Evaluation. *J. Eng. Fibers Fabr.* **2015**, 155892501501000401.
(30) Ju, J.; Zheng, Y.; Jiang, L. Bioinspired one-dimensional materials for directional liquid transport. *Acc. Chem. Res.* **2014**, *47*, 2342−2352.
(31) Liu, C.; Xue, Y.; Chen, Y.; Zheng, Y. Effective directional self-gathering of drops on spine of cactus with splayed capillary arrays. *Sci. Rep.* **2015**, *5*, 17757.
(32) Sharma, V.; Sharma, M.; Kumar, S.; Krishnan, V. Investigations on the fog harvesting mechanism of Bermuda grass (Cynodon dactylon). *Flora* **2016**, *224*, 59−65.
(33) Peng, Y.; He, Y.; Yang, S.; Ben, S.; Cao, M.; Li, K.; Liu, K.; Jiang, L. Magnetically Induced Fog Harvesting via Flexible Conical Arrays. *Adv. Funct. Mater.* **2015**, *25*, 5967−5971.
(34) Chen, D.; Li, J.; Zhao, J.; Guo, J.; Zhang, S.; Sherazi, T. A.; Ambreen; Li, S. Bioinspired superhydrophilic-hydrophobic integrated surface with conical pattern-shape for self-driven fog collection. *J. Colloid Interface Sci.* **2018**, *530*, 274−281.
(35) Seo, D.; Lee, J.; Lee, C.; Nam, Y. The effects of surface wettability on the fog and dew moisture harvesting performance on tubular surfaces. *Sci. Rep.* **2016**, *6*, 24276.
(36) Lalia, B. S.; Anand, S.; Varanasi, K. K.; Hashaikeh, R. Fog-harvesting potential of lubricant-impregnated electrospun nanomats. *Langmuir* **2013**, *29*, 13081−13088.
(37) Upadhyay, R. K.; Waghmare, P. R. Green preparation of copper surfaces with wettability contrast for guided fluid transport and fog harvesting application. *Mater. Lett.* **2019**, *246*, 223−226.
(38) Caldas, L.; Andaloro, A.; Calafiore, G.; Munechika, K.; Taube, B.; Oliveira, M.; Cabrini, S. Water harvesting from fog using building envelopes: part II. *Water Environ. J.* **2018**, *32*, 466−475.
(39) Azad, M. A. K.; Ellerbrok, D.; Barthlott, W.; Koch, K. Fog collecting biomimetic surfaces: Influence of microstructure and wettability. *Bioinspiration Biomimetics* **2015**, *10*, No. 016004.
(40) Sharma, V.; Balaji, R.; Krishnan, V. Fog-Harvesting Properties of Dryopteris marginata: Role of Interscalar Microchannels in Water-Channeling. *Biomimetics* **2018**, *3*, 7.
(41) Su, Y.; Cai, S.; Wu, T.; Li, C.; Huang, Z.; Zhang, Y.; Wu, H.; Hu, K.; Chen, C.; Li, J.; Hu, Y.; Zhu, S.; Wu, D. Smart Stretchable Janus Membranes with Tunable Collection Rate for Fog Harvesting. *Adv. Mater. Interfaces* **2019**, *6*, 1901465.
(42) Yang, X.; Song, J.; Liu, J.; Liu, X.; Jin, Z. A Twice Electrochemical-Etching Method to Fabricate Superhydrophobic-Superhydrophilic Patterns for Biomimetic Fog Harvest. *Sci. Rep.* **2017**, *7*, 8816.
(43) Park, K.-C.; Chhatre, S. S.; Srinivasan, S.; Cohen, R. E.; McKinley, G. H. Optimal design of permeable fiber network structures for fog harvesting. *Langmuir* **2013**, *29*, 13269−13277.
(44) Labbé, R.; Duprat, C. Capturing aerosol droplets with fibers. *Soft Matter* **2019**, *15*, 6946−6951.
(45) Bai, H.; Tian, X.; Zheng, Y.; Ju, J.; Zhao, Y.; Jiang, L. Direction controlled driving of tiny water drops on bioinspired artificial spider silks. *Adv. Mater.* **2010**, *22*, 5521−5525.
(46) Lorenceau, L.; Quéré, D. Drops on a conical wire. *J. Fluid Mech.* **2004**, *510*, 29−45.
(47) Kawasaki, K. Study of wettability of polymers by sliding of water drop. *J. Colloid Sci.* **1960**, *15*, 402−407.
(48) Lee, A.; Moon, M.-W.; Lim, H.; Kim, W.-D.; Kim, H.-Y. Water harvest via dewing. *Langmuir* **2012**, *28*, 10183−10191.
(49) Protiere, S.; Duprat, C.; Stone, H. A. Wetting on two parallel fibers: drop to column transitions. *Soft Matter* **2013**, *9*, 271−276.
(50) Lee, S.-W.; Laibinis, P. E. Directed Movement of Liquids on Patterned Surfaces Using Noncovalent Molecular Adsorption. *J. Am. Chem. Soc.* **2000**, *122*, 5395−5396.
(51) Bai, H.; Wang, L.; Ju, J.; Sun, R.; Zheng, Y.; Jiang, L. Efficient water collection on integrative bioinspired surfaces with star-shaped wettability patterns. *Adv. Mater.* **2014**, *26*, 5025−5030.

https://dx.doi.org/10.1021/acsomega.0c05776
ACS Omega 2021, 6, 3910−3920

(52) Tan, X.; Zhu, Y.; Shi, T.; Tang, Z.; Liao, G. Patterned gradient surface for spontaneous droplet transportation and water collection: simulation and experiment. *J. Micromech. Microeng.* **2016**, *26*, 115009.
(53) Yao, X.; Bai, H.; Ju, J.; Zhou, D.; Li, J.; Zhang, H.; Yang, B.; Jiang, L. Running droplet of interfacial chemical reaction flow. *Soft Matter* **2012**, *8*, 5988.
(54) Yang, S.; Yin, K.; Chu, D.; He, J.; Duan, J.-A. Femtosecond laser structuring of Janus foam: Water spontaneous antigravity unidirectional penetration and pumping. *Appl. Phys. Lett.* **2018**, *113*, 203701.
(55) Zhang, S.; Huang, J.; Chen, Z.; Yang, S.; Lai, Y. Liquid mobility on superwettable surfaces for applications in energy and the environment. *J. Mater. Chem. A* **2019**, *7*, 38−63.
(56) Carroll, B. J. The Accurate Measurement of Contact Angle, Phase Contact Areas, Drop Volume, and Laplace Excess Pressurein Drop-on-Fiber Systems. *J. Colloid Interface Sci.* **1976**, *57*, 488−495.
(57) Ju, J.; Xiao, K.; Yao, X.; Bai, H.; Jiang, L. Bioinspired conical copper wire with gradient wettability for continuous and efficient fog collection. *Adv. Mater.* **2013**, *25*, 5937−5942.
(58) Ju, J.; Yao, X.; Yang, S.; Wang, L.; Sun, R.; He, Y.; Jiang, L. Cactus Stem Inspired Cone-Arrayed Surfaces for Efficient Fog Collection. *Adv. Funct. Mater.* **2014**, *24*, 6933−6938.
(59) Zheng, Y.; Bai, H.; Huang, Z.; Tian, X.; Nie, F. Q.; Zhao, Y.; Zhai, J.; Jiang, L. Directional water collection on wetted spider silk. *Nature* **2010**, *463*, 640−643.
(60) McHale, G.; Newton, M. I. Global geometry and the equilibrium shapes of liquid drops on fibers. *Colloids Surf., A* **2002**, *206*, 79−86.
(61) Wu, J.; Yin, K.; Li, M.; Wu, Z.; Xiao, S.; Wang, H.; Duan, J.-A.; He, J. Under-oil self-driven and directional transport of water on femtosecond laser-processed superhydrophilic geometry-gradient structure. *Nanoscale* **2020**, *12*, 4077−4084.
(62) Azeem, M.; Guérin, A.; Dumais, T.; Caminos, L.; Goldstein, R. E.; Pesci, A. I.; de Dios Rivera, J.; Torres, M. J.; Wiener, J.; Campos, J. L.; Dumais, J. Optimal Design of Multilayer Fog Collectors. *ACS Appl. Mater. Interfaces* **2020**, *12*, 7736−7743.
(63) de Dios Rivera, J. Aerodynamic collection efficiency of fog water collectors. *Atmos. Res.* **2011**, *102*, 335−342.

https://dx.doi.org/10.1021/acsomega.0c05776
ACS Omega 2021, 6, 3910−3920